forum acusticum 2026
8-12 September · Graz, Austria

WHY 2.5D SOUND FIELD SYNTHESIS ISN'T GOING TO PRODUCE DIFFUSE SOUND FIELDS WELL ENOUGH

Franz Zotter, Lukas Gölles, Matthias Frank

Institute of Electronic Music and Acoustics, University of Music and Performing Arts Graz, Austria

This paper is a revised version of the authors' submitted manuscript that was peer-reviewed by at least two anonymous reviewers.

Abstract

Reproducing surround audio via a horizontal ring of 3D point-source loudspeakers is termed 2.5D synthesis. Such layouts were recently proven incapable of producing spatially extended diffuse sound fields when fed with mutually uncorrelated signals. *Could feeding the loudspeakers via 2.5D sound field synthesis help?* We show that the horizontal ring layout of vertical line sources is the ideal 2D layout and permits full control with convolutional driving functions. Such functions are general enough to also include 2.5D WFS or 2.5D Ambisonics with spectral division. But no convolutional driving function can help a 2.5D layout synthesize extended diffuse fields from uncorrelated input. While active sound intensity must vanish in the ideal diffuse field, convolutional driving functions for 2.5D inevitably produce net inward sound intensity.

Keywords: *diffuse sound fields, 2.5d wave-field synthesis, higher-order ambisonics, sound-field synthesis*

1. Introduction

Theories of sound field synthesis can be found in Ahrens' textbook [1], Fazi et al. [2], and the Handbook of Audio technology [3] (to appear in English soon). Wave-field synthesis dates back to Berkhout [4], Start [5], and Ambisonic synthesis was described by Ward et al. [6] and Daniel [7]. Some of the work has been fueled by the ability to produce precise replicas of wave fields. Perceptual aspects were covered by Wierstorf [8], and a summary provided by Spors et al. [9]. Investigations on the required number of plane waves for a perceptually diffuse sound field were carried out by Sonke et al. [10] and Ahrens [11].

An ideal diffuse sound field should, independently of position and direction, exhibit: (i) a uniform sound-pressure level, (ii) vanishing active sound intensity, (iii) a distance-dependent sound pressure correlation, and (iv) an isotropic sectorial sound intensity. These properties are addressed in recent works by Riedel et al. [12], Zotter et al. [13], [14], and Tanaka et al. [15]–[17], with vanishing ILD/active intensity identified as the main challenge when synthesizing perceptually balanced 2D diffuse sound fields [12], [14], necessitating true plane-wave or vertical-line-source loudspeakers. Whether 2.5D synthesis could help remained untested.

Experiments by Melchior et al. [18] found that 2.5D-WFS synthesized diffuse fields become unidirectional when reference lines are displaced from the listening position. Zotter et al.'s preprint [19] showed that, for a central listening position, 2.5D WFS produces vanishing active intensity only there, not throughout the synthesis area. It found no clear benefit in varying the virtual source distance from infinite to focused.

Our present paper is dedicated to addressing this 2.5D sound field synthesis issue. In this regard, it would be desirable to clarify more generally whether there can be a synthesis method capable of producing 2D diffuse sound fields using a horizontal ring of 3D point sources. We will assume that typical 2.5D driving functions have a shift-invariant shape with regard to any virtual sound direction. This assumption should hold for focused or distant virtual sources, regardless of whether 2.5D WFS or 2.5D Ambisonics with spectral division is the chosen method, or something beyond. In this paper, we will use *convolutional* to refer to such a circular convolution on the azimuth angle.

To this end, we formulate the driving function as a circular convolution kernel. We investigate a horizontal ring arrangement of infinite vertical line sources as ideal synthesis case followed by the sub-optimal point-source arrangement on a horizontal ring, so that we can demonstrate what the kernel can and cannot control. We show that (i) with 2D line sources, the active sound intensity is forced to zero everywhere, and plane-wave weights flatten the sound energy density, while (ii) with 3D point sources, even with optimized driving function weights (via non-negative least squares up to $r \le 0.75\, r_\mathrm{s}$), energy can only be partially flattened and active sound intensity can't be annihilated, Figure 1.

Corresponding author: *zotter@iem.at.*

2. Sound Field Synthesis with a horizontal ring of loudspeakers

Sound field synthesis methods using a circular array, be it horizontal Ambisonics or WFS, can be commonly described to utilize a driving function $K(\varphi_\mathrm{s}-\varphi_\mathrm{v})$ that distributes a single virtual-source signal $q(\varphi_\mathrm{v})$ from the virtual source angle φ_v at some radius r_v to every angle φ_s on the surrounding loudspeaker ring, with the radius r_s. At some frequency ω or wave number $k=\frac{\omega}{c}$, the driving function of a virtual source is a complex-valued convolution kernel $K\in\mathbb{C}$, yielding the angular signal for a single virtual source at φ_v,

$$x_\mathrm{single}(\varphi_\mathrm{s}) = K(\varphi_\mathrm{s}-\varphi_\mathrm{v})\,q(\varphi_\mathrm{v}), \tag{1}$$

of the virtual-source signal $q(\varphi_\mathrm{v})$. Diffuse sound fields integrate simultaneous virtual sources across all angles

$$x(\varphi_\mathrm{s}) = \int K(\varphi_\mathrm{s}-\varphi_\mathrm{v})\,q(\varphi_\mathrm{v})\,\mathrm{d}\varphi_\mathrm{v}. \tag{2}$$

The resulting angular signal $x(\varphi_\mathrm{s})$ drives the loudspeakers modeled by Green's functions $G(r,r_\mathrm{s},\varphi-\varphi_\mathrm{s})$. We observe their sound pressure p and radial sound-particle velocity v_r at the angle φ and radius r,

$$p(r,\varphi) = \int G(r,r_\mathrm{s},\varphi-\varphi_\mathrm{s})\,x(\varphi_\mathrm{s})\,\mathrm{d}\varphi_\mathrm{s}, \tag{3}$$

$$\rho\,c\,v_\mathrm{r}(\varphi) = \mathrm{i}\int \frac{\partial}{\partial kr}G(r,r_\mathrm{s},\varphi-\varphi_\mathrm{s})\,x(\varphi_\mathrm{s})\,\mathrm{d}\varphi_\mathrm{s}. \tag{4}$$

All integrals above are circular convolutions: q convolved with K convolved either with G or $\frac{\partial}{\partial kr}G$. In the angular Fourier expansion $e^{\mathrm{i}m\varphi}$ with regard to the observed angle φ, this simplifies to a multiplication of the individual angular Fourier coefficients γ_m, $\gamma_{\mathrm{r},m}$, κ_m, and ϕ_m of G, $\frac{\partial}{\partial kr}G$, K, and q, respectively,

$$p(\varphi) = \sum_{m=-\infty}^{\infty} \gamma_m\,\kappa_m\,\phi_m\,e^{\mathrm{i}m\varphi}, \tag{5}$$

$$\rho\,c\,v_\mathrm{r}(\varphi) = \sum_{m=-\infty}^{\infty} \mathrm{i}\,\gamma_{\mathrm{r},m}\,\kappa_m\,\phi_m\,e^{\mathrm{i}m\varphi}. \tag{6}$$

For diffuse sound field synthesis, we assume uniform-variance virtual-source signals $q(\varphi)$ without correlation $E\{q^*(\varphi_1)\,q(\varphi_2)\}=\frac{1}{2\pi}\delta(\varphi_1-\varphi_2)$. This translates to $E\{\phi_m^*\,\phi_n\}=\delta_{m,n}$ for their Fourier coefficients. We use this restriction to diffuse fields whose azimuthal modes are mutually uncorrelated throughout, so that second-order quantities depend on $|\kappa_m|^2$ only. Potential sound-energy density $w=E\{|p|^2\}/2\rho c^2$ and radial active sound intensity $I_\mathrm{r}=\Re\{E\{p^* v_\mathrm{r}\}\}$ define

$$2\rho c^2 w = \sum_{m,n}\gamma_m^*\kappa_m^*\gamma_n\kappa_n E\{\phi_m^*\phi_n\} = \sum_m |\gamma_m|^2|\kappa_m|^2, \tag{7}$$

$$\rho c\,I_\mathrm{r} = -\sum_m \Im\{\gamma_m^*\gamma_{\mathrm{r},m}\}\,|\kappa_m|^2; \tag{8}$$

note the leading i in (6) turned $\Re\{\cdot\}$ into $-\Im\{\cdot\}$ above. This means that sound field synthesis by any driving function K decomposed into Fourier coefficients $\kappa_m\in\mathbb{C}$ is able to scale by the magnitude squares $|\kappa_m|^2$ the r-dependent mode strengths $|\gamma_m|^2$ of sound energy density and $-\Im\{\gamma_m^*\gamma_{\mathrm{r},m}\}$ of radial sound intensity.

2.1. Why 2D Sound Field Synthesis works: 2D Green's functions on a circle

When placed at $(r_\mathrm{s},0)$ and observed at (r,φ) in polar coordinates, one single vertical line source (2D Green's function) $\frac{1}{4\mathrm{i}}H_0^{(2)}(kR)$ is evaluated at $R=\sqrt{r^2-2rr_\mathrm{s}\cos\varphi+r_\mathrm{s}^2}$. Its addition theorem $H_0^{(2)}(kR)=\sum_m J_m(kr)H_m^{(2)}(kr_\mathrm{s})e^{\mathrm{i}m\varphi}$ [20, (10.23.7)], $r\le r_\mathrm{s}$, defines the mode strengths γ_m^2D that we need,

$$G_\mathrm{2D}(r,r_\mathrm{s},\varphi) = \tfrac{1}{4\mathrm{i}}\sum_{m=-\infty}^{\infty} J_m(kr)\,H_m^{(2)}(kr_\mathrm{s})\,e^{\mathrm{i}m\varphi},$$
$$\Rightarrow \gamma_m^\mathrm{2D} = \tfrac{1}{4\mathrm{i}}J_m(kr)\,H_m^{(2)}(kr_\mathrm{s})\,. \tag{9}$$

The normalized energy density in (7) yields with γ_m^2D

$$2\rho c^2 w = \tfrac{1}{16}\sum_m J_m^2(kr)\,|H_m^{(2)}(kr_\mathrm{s})|^2\,|\kappa_m|^2. \tag{10}$$

With an m-independent factor $|\kappa_m|^2=8\pi\,kr_\mathrm{s}$ as in Figure 1a (top) for the example $kr_\mathrm{s}=5$, energy density is only flat around 0 and increases toward r_s.
To synthesize every $q(\varphi_\mathrm{v})$ as a plane wave, we need

$$\kappa_m = \frac{4\,\mathrm{i}^{m+1}}{H_m^{(2)}(kr_\mathrm{s})}, \tag{11}$$

which matches energy density uniformly with an ideal 2D diffuse field, cf. Figure 1b (top) and [20, (10.23.3)],

$$2\rho c^2 w = \sum_{m=-\infty}^{\infty} J_m^2(kr) = 1. \tag{12}$$

Active intensity (8) uses the radial derivative of γ_m^2D,

$$\tfrac{\partial}{\partial kr}G_\mathrm{2D}(r,r_\mathrm{s},\varphi) = \tfrac{1}{4\mathrm{i}}\sum_{m=-\infty}^{\infty} J_m'(kr)\,H_m^{(2)}(kr_\mathrm{s})\,e^{\mathrm{i}m\varphi},$$
$$\Rightarrow \gamma_{\mathrm{r},m}^\mathrm{2D} = \tfrac{1}{4\mathrm{i}}J_m'(kr)\,H_m^{(2)}(kr_\mathrm{s})\,, \tag{13}$$

and it makes the normalized radial active sound intensity in (8) vanish uniformly for any choice of κ_m

$$\rho\,c\,I_\mathrm{r} = -\sum_m \Im\big\{\tfrac{J_m\,J_m'\,|H_m^{(2)}|^2|\kappa_m|^2}{16}\big\} \equiv 0\,. \tag{14}$$

The expression $\frac{J_m\,J_m'\,|H_m^{(2)}|^2|\kappa_m|^2}{16}$ is real-valued for any $|\kappa_m|^2, kr, kr_\mathrm{s}\in\mathbb{R}^+$, $0\le kr\le kr_\mathrm{s}$, so $\Im\{\cdot\}$ vanishes.
This ideal result relied on the mutual uncorrelatedness of the signals ϕ_m, which led to the real-valued, hence vanishing imaginary part, here, see also Figure 1a (bottom) and Figure 1b (bottom).

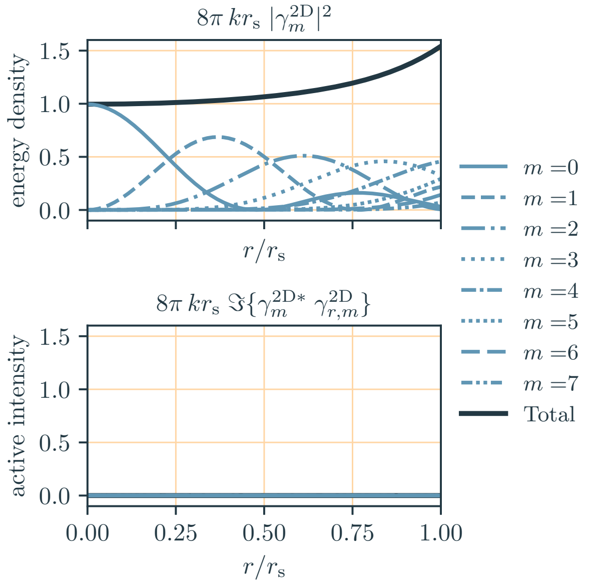

(a) 2D ring, constant $|\kappa_m|^2$: energy flat near 0, intensity vanishes.

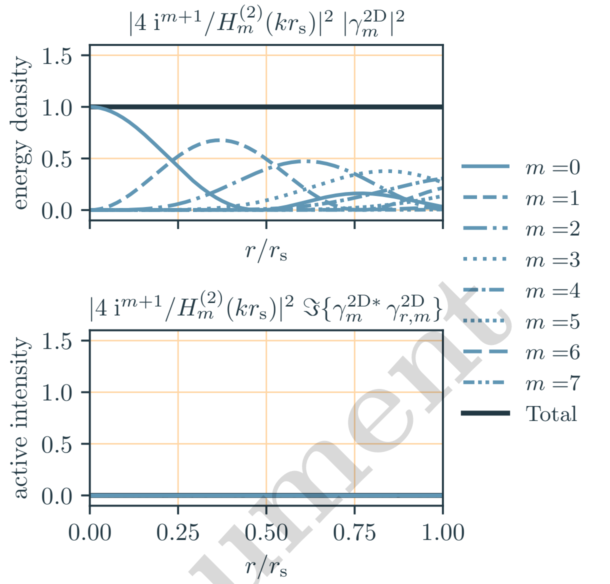

(b) 2D ring, plane-wave $|\kappa_m|^2$: energy flat, intensity vanishes.

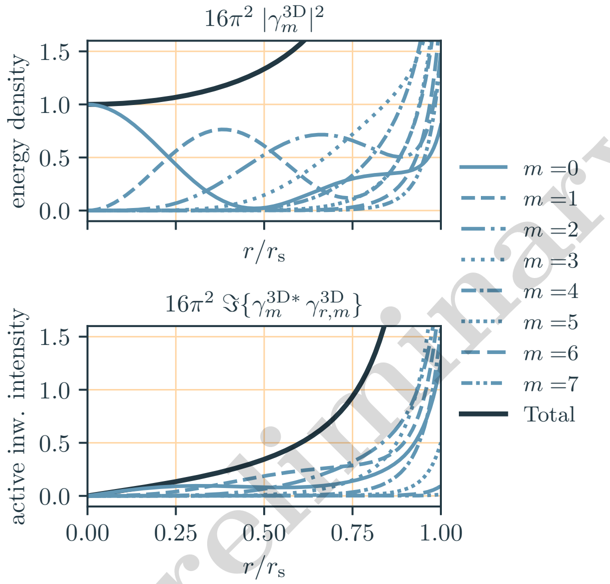

(c) 3D ring, $|\kappa_m|^2 = 16\pi^2$: energy and intensity rise toward r_s.

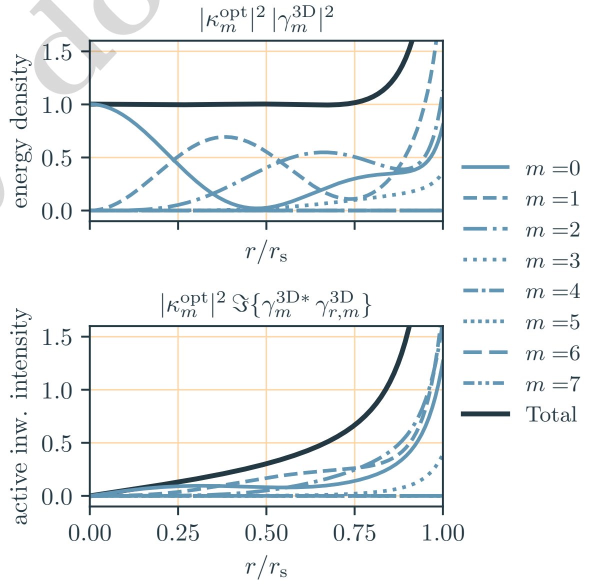

(d) 3D ring, NNLS $|\kappa_m^{\mathrm{opt}}|^2$ flattened energy toward $0.75 r_\mathrm{s}$, intensity remains.

Figure 1: Diffuse sound field synthesis with horizontal ring in terms of modal/total potential sound energy density (top in each subplot) and modal/total negative radial active intensity (bottom in each subplot) for 2D and 3D source rings at $kr_\mathrm{s} = 5$ in each subfigure. Top subplots a, b: 2D with constant (left) vs. plane-wave weights (right). Bottom subplots c, d: 3D with constant $|\kappa_m|^2$ (left) vs. NNLS $|\kappa_m^{\mathrm{opt}}|^2$ for flat energy density $r \leq 0.75 r_\mathrm{s}$ (right); only 2D source ring (vertical line sources) yields uniformly flat energy and vanishing intensity. Note that only the 3D cases exhibit this particular inward active intensity $I_\mathrm{r} \leq 0$ due to off-diagonal spherical-order index pairs $l \neq n$ in the second-order statistics.

2.2. Why 2.5D Sound Field Synthesis doesn't work: 3D Green's functions on a circle

The mode strength $\gamma_m^{3\mathrm{D}}$ of a single point source $\frac{e^{-\mathrm{i}kR}}{4\pi R}$ (3D Green's function) placed at the spherical radius r_s, azimuth $\varphi_\mathrm{s} = 0$, and zenith $\vartheta_\mathrm{s} = \frac{\pi}{2}$ (horizon), and observed at $(r, \varphi, \frac{\pi}{2})$, hence $R = \sqrt{r^2 - 2rr_\mathrm{s}\cos\varphi + r_\mathrm{s}^2}$, is obtained from the addition theorems [20, (10.60.3)] [20, (14.30.9)], $r \leq r_\mathrm{s}$,

$$G_{3\mathrm{D}}(r,r_\mathrm{s},\varphi) = \\ -\mathrm{i}k \sum_{n,m} Y_n^m(\varphi, \tfrac{\pi}{2})\, Y_n^{m*}(0, \tfrac{\pi}{2})\, j_n(kr)\, h_n^{(2)}(kr_\mathrm{s}). \tag{15}$$

For the complex-valued spherical harmonics $Y_n^m(\varphi, \vartheta)$ one can extract the azimuth harmonic by writing $Y_n^m(\varphi, \frac{\pi}{2}) = Y_n^m(0, \frac{\pi}{2})\, e^{\mathrm{i}m\varphi}$, so that we get $\gamma_m^{3\mathrm{D}}$

$$\gamma_m^{3\mathrm{D}} = -\mathrm{i}k \sum_{n=|m|}^{\infty} \beta_n^{|m|}\, j_n(kr)\, h_n^{(2)}(kr_\mathrm{s}), \tag{16}$$

with the explicit magnitude square $\beta_n^{|m|}$ of the harmonic

$$\beta_n^{|m|} = \left|Y_n^m(0, \tfrac{\pi}{2})\right|^2 = \tfrac{(2n+1)(n-|m|)!}{4\pi\,(n+|m|)!}\,[P_n^{|m|}(0)]^2. \tag{17}$$

For normalized energy density (7), $\gamma_m^{3\mathrm{D}}$ yields

$$2\rho c^2 w = k^2 \sum_m |\kappa_m|^2 \times \\ \sum_{l,n} \beta_l^{|m|}\beta_n^{|m|} j_l(kr) j_n(kr) h_l^{(2)*}(kr_\mathrm{s}) h_n^{(2)}(kr_\mathrm{s}), \tag{18}$$

where the double sum runs over the spherical orders $l, n \geq |m|$. The result is real-valued: for any l, n the reverse n, l exists, with identical real-valued factors but conjugate imaginary parts that cancel $h_l^{(2)*} h_n^{(2)} + h_n^{(2)*} h_l^{(2)}$ as in any sum of complex conjugates, $f + f^* \in \mathbb{R}$. The result for the $kr_\mathrm{s} = 5$ example is shown in Figure 1c (top) for $|\kappa_m|^2 = 16\pi^2$ and a non-negative least-squares optimum $|\kappa_m^{\mathrm{opt}}|^2$ for a flat energy density up to $r \leq 0.75 r_\mathrm{s}$ is shown in Figure 1d (top). Both cases show an increase in energy density toward r_s.
For the sound intensity, the radially derived source coefficients are given by

$$\gamma_{\mathrm{r},m}^{3\mathrm{D}} = -\mathrm{i}k \sum_{n=|m|}^{\infty} \beta_n^{|m|} j_n'(kr)\, h_n^{(2)}(kr_\mathrm{s}), \tag{19}$$

which yields the normalized radial active intensity (8)

$$\rho\, c\, I_\mathrm{r} = -k^2 \sum_m |\kappa_m|^2 \times \\ \sum_{l,n} \beta_l^{|m|}\beta_n^{|m|} j_l(kr) j_n'(kr)\; \Im\{h_l^{(2)*}(kr_\mathrm{s}) h_n^{(2)}(kr_\mathrm{s})\} \\ = \sum_m \tfrac{k^2|\kappa_m|^2}{2} \sum_{l,n} \beta_l^{|m|}\beta_n^{|m|}\, A_l^n(kr)\, B_l^n(kr_\mathrm{s}), \tag{20}$$

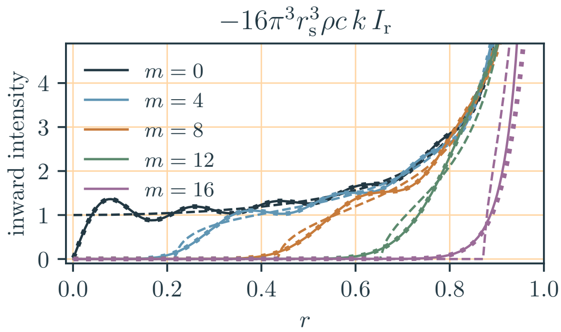

Figure 2: Radial inward intensities $-I_\mathrm{r}$ for $r_\mathrm{s} = 1\,\mathrm{m}$, $f = 1\,\mathrm{kHz}$, $m = 0, 4, \ldots, \lceil kR \rceil$, normalized with $16\pi^3 r_\mathrm{s}^3\, \rho c\, k$: stationary-phase approximation (dashed) vs. numerical integral (solid), and analytic double sum (dotted).

$$\text{with } A_l^n(kr) = j_l(kr) j_n'(kr) - j_l'(kr) j_n(kr) \tag{21} \\ \text{and } B_l^n(kr_\mathrm{s}) = j_l(kr_\mathrm{s}) y_n(kr_\mathrm{s}) - y_l(kr_\mathrm{s}) j_n(kr_\mathrm{s}).$$

In the real-valued product, both terms $A_l^n = -A_n^l$, $B_l^n = -B_n^l$ are anti-symmetric with index transposition $l \leftrightarrow n$, so that the diagonal $A_l^l = B_l^l = 0$ vanishes and the product is symmetric $A_l^n B_l^n = A_n^l B_n^l$. The active radial intensity I_r is negative (inward) for $kr > 0$

$$\sum_{l,n} \beta_l^{|m|}\beta_n^{|m|} A_l^n(kr)\, B_l^n(kr_\mathrm{s}) < 0, \quad 0 < kr < kr_\mathrm{s}.$$

For $|\kappa_m|^2 = 16\pi^2$ as in Figure 1c (bottom), this agrees with [13]; but even NNLS-optimized weights ($|\kappa_m^{\mathrm{opt}}|^2 \geq 0$) in Figure 1d (bottom) leave a non-zero intensity. Figure 2 displays the strictly inward-oriented intensity at any $0 < kr < kr_\mathrm{s}$ for individual modes m.

2.2.1. Numerical proof and discussion

Lacking an analytic proof of negative sound intensity, a numerical validation was carried out via the MATLAB script `test_negativity.m` at https://git.iem.at/zotter/2026-fa2026-2.5dsfs. It samples kr_s in 15 log-spaced steps between 10^{-4} and 10^3, as well as 51 log-spaced steps for kr between $10^{-3}\, kr_\mathrm{s}$ and kr_s, for all $0 \leq m \leq 19$ with $n_{\max}$ adapted to $\lceil 1.2\, kr_\mathrm{s} \rceil$. No non-negative intensity case was found among the 15 300 tested (kr, kr_s) samples.
Figure 2 verifies the result of the analytic double sum eq. (20) (dotted) against $I_\mathrm{r} = \Re\{p^* v_\mathrm{r}\}$ obtained from integrating an angular mode $e^{\mathrm{i}m\varphi_\mathrm{s}}$ via summation over 300 uniformly spaced Green's functions, cf. eq. (22). The match is precise at the example modes $m = 0, 4, 8, 12, 16$ and confirms the net inward intensity.
These are significant results because net inward intensity can never vanish for uncorrelated or individual 2D modes unless $kr = 0$. Even worse: vanishing intensity can't be enforced by non-negative modal weights $|\kappa_m|^2$, because these can't change the sign of the negative off-diagonal contributions in the l, n double sum. Any linear combination over m inevitably accumulates inward intensity rather than allowing destructive interference.

This result is independent of the particular 2.5D correction employed, provided that the driving function is convolutional and shift-invariant with respect to the azimuth angle, an assumption common to all standard horizontal sound field synthesis formulations.

2.2.2. Stationary-phase approximation at a single m

Stationary-phase approximation provides analytic evaluation of integrals and insights into the per-mode imbalance; what follows condenses the detailed supplementary derivation in `stationary_phase.pdf` at https://git.iem.at/zotter/2026-fa2026-2.5dsfs.

The angular Fourier coefficient γ_m^{3D} equals the Green's function $G = \frac{e^{-\mathrm{i}kR}}{4\pi\,R}$ integrated over a normalized mode $\frac{1}{2\pi}e^{\mathrm{i}mx}$. The observer is shifted to r along the radial at the zero polar angle $\varphi = 0$, and $x \equiv \varphi_{\mathrm{s}}$ denotes the global polar angle of the source, to keep the notation of differential elements simple, so that we get:

$$p = \gamma_m^{\mathrm{3D}} = \frac{1}{2\pi}\int_{-\pi}^{\pi} \frac{e^{-\mathrm{i}kR+\mathrm{i}mx}}{4\pi\,R}\,\mathrm{d}x. \qquad (22)$$

Here $\phi = mx - kR$ is the phase of the integrand. The distance $R = \sqrt{r^2 - 2rr_{\mathrm{s}}\cos x + r_{\mathrm{s}}^2}$ alone has extrema at $x = 0, \pi$ and increases on $x \in [0, \pi]$ for any $r > 0$. Altogether for $kr > |m|$, the phase $\phi = mx - kR$ is stationary $\phi' = 0$ only at the angles x_0 near 0 and x_π near π that accordingly satisfy $-\frac{kr\,r_{\mathrm{s}}\sin x}{R} + m = 0$. The relation between the global polar source angle x and observed local source angle α via $r_{\mathrm{s}}\sin x = R\sin\alpha$ yields stationary phase at

$$\sin\alpha_{0,\pi} = \frac{m}{kr}, \qquad (23)$$

cf. Figure 3. Each of the corresponding stationary points $x_{0,\pi}$ of $r_{\mathrm{s}}\sin x_{0,\pi} = R_{0,\pi}\sin\alpha_{0,\pi}$ contributes to sound pressure

$$p_{0,\pi} = \frac{1}{8\pi^2}\sqrt{\frac{2\pi}{|\phi''|_{0,\pi}}}\,\frac{e^{\mathrm{i}\phi_{0,\pi}+\mathrm{i}\frac{\pi}{4}\mathrm{sgn}\{\phi''_{0,\pi}\}}}{R_{0,\pi}}, \qquad (24)$$

and approximate pressure and particle velocity become

$$p \approx p_0 + p_\pi, \qquad \lim_{kR\gg 1} v_{\mathrm{r}} \approx \frac{\cos\alpha_0}{\rho\,c}\left[-p_0 + p_\pi\right]. \qquad (25)$$

Near-field contributions to v_{r} are purely reactive and vanish in $I_{\mathrm{r}} = \Re\{p^* v_{\mathrm{r}}\}$ so that the far-field $\lim_{kR\gg 1} v_{\mathrm{r}}$ is accurate. The slope $\phi' = m - kr\sin\alpha$, curvature $\phi'' = -\frac{kr\,\cos\alpha}{R}\frac{S}{2}$ with $S = 2r_{\mathrm{s}}\sqrt{1 - \frac{m^2}{k^2 r_{\mathrm{s}}^2}}$, and approximation in eq. (24) are derived step-by-step in the supplementary material. The resulting net sound intensity approximation I_{r} is negative for $kr > |m|$:

$$I_{\mathrm{r}} = \Re\{p^* v_{\mathrm{r}}\} \approx \frac{1}{16\pi^3\rho c\,krS}\left[-\frac{1}{R_0} + \frac{1}{R_\pi}\right] < 0. \qquad (26)$$

It is dominated by the inward flux from the nearer side $R_0 < R_\pi$, cf. Figure 3.

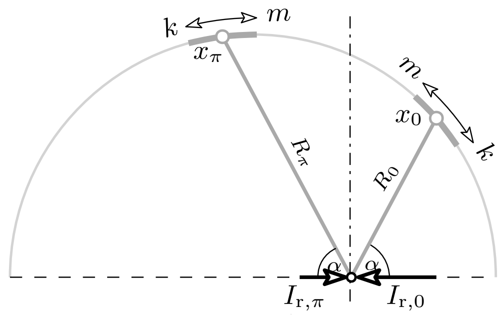

Figure 3: Geometry: stationary-phase approximation.

Figure 2 validates the stationary-phase result (dashed) against eq. (20) (dotted) and discretized eq. (22). Unlike these precise representations, as expected, stationary phase approximation captures the smooth trend without oscillations, as soon as kr lies well above $|m|$. The reciprocal radii in eq. (26) reveal the fundamental geometric imbalance for $kr > |m|$: intensity is always dominated by the negative contribution of the distance R_0 to the nearer stationary-phase point.
Otherwise at $kr < |m|$, the synthesized field is evanescent: the integrand does not exhibit stationary-phase points, so not only p but also v_{r} vanish and with them $I_{\mathrm{r}} \approx 0$, which represents the balanced silence of the evanescent field rather than a balanced diffuse field.

3. Conclusion

With the common assumption of a convolutional driving function and mutually uncorrelated isotropic azimuthal excitation, a horizontal ring of 3D point sources can't synthesize an isotropic 2D diffuse sound field with both uniform sound pressure level and uniformly vanishing radial active intensity. By contrast, vertical line sources (2D Green's functions) can.
Compared to the numerical simulations in [19], the results are more general: no convolutional driving function can suppress the net inward intensity, neither by non-negative least-squares, nor by 2.5D Ambisonics or 2.5D WFS, nor by any other shift-invariant method. This covers, in particular, varying the virtual source distance between plane-wave and focused. The underlying imbalance is fundamental, confirmed by numerical simulations, and explained by stationary-phase approximation.
Sources used to generate the plots, numerical validation, and the article itself are made available at https://git.iem.at/zotter/2026-fa2026-2.5dsfs for reproducible research.

References

[1] J. Ahrens, *Analytic methods of sound field synthesis*. Springer, 2012. [Online]. Available: `https://doi.org/10.1007/978-3-642-25743-8`.

[2] F. M. Fazi and P. A. Nelson, "Sound field reproduction as an equivalent acoustical scattering problem," *The Journal of the Acoustical Society of America*, vol. 134, no. 5, pp. 3721–3729, Nov.

2013. [Online]. Available: https://doi.org/10.1121/1.4824343.

[3] F. Schultz, N. Hahn, and S. Spors, "Wellenfeldsynthese," in *Handbuch der Audiotechnik*, S. Weinzierl, Ed. Berlin, Heidelberg: Springer, 2025, pp. 595–614. [Online]. Available: https://doi.org/10.1007/978-3-662-60369-7_26.

[4] A. Berkhout, D. de Vries, and P. Vogel, "Acoustic control by wave field synthesis," *JASA*, vol. 93, no. 5, pp. 2764–2778, 1993. [Online]. Available: https://doi.org/10.1121/1.405852.

[5] E. W. Start, "Direct sound enhancement using wave field synthesis," Ph.D. dissertation, TU Delft, 1997. [Online]. Available: https://repository.tudelft.nl/islandora/object/uuid:c80d5b58-67d3-4d84-9e73-390cd30bde0d/datastream/OBJ/download.

[6] D. Ward and T. Abhayapala, "Reproduction of a plane-wave sound field using an array of loudspeakers," *IEEE TSAP*, vol. 9, no. 6, pp. 697–707, 2001. [Online]. Available: https://doi.org/10.1109/89.943347.

[7] J. Daniel, "Représentation de champs acoustiques, application à la transmission et à la reproduction de scènes sonores complexes dans un contexte multimédia," Ph.D. dissertation, Université de Paris 6, 2001. [Online]. Available: http://gyronymo.free.fr/audio3D/downloads/These-original-version.zip.

[8] H. Wierstorf, "Perceptual assessment of sound field synthesis," Ph.D. dissertation, TU Berlin, 2014. [Online]. Available: https://doi.org/10.14279/depositonce-4310.

[9] S. Spors, H. Wierstorf, A. Raake, F. Melchior, M. Frank, and F. Zotter, "Spatial sound with loudspeakers and its perception: A review of the current state," *Proc. IEEE*, vol. 101, no. 9, pp. 1920–1938, 2013. DOI: 10.1109/JPROC.2013.2264784. [Online]. Available: https://doi.org/10.1109/JPROC.2013.2264784.

[10] J.-J. Sonke and D. de Vries, "Generation of diffuse reverberation by plane wave synthesis," in *102nd AES Conv*, Munich, Mar. 1997. [Online]. Available: https://aes.org/publications/elibrary-page/?id=7324.

[11] J. Ahrens, "Perceptual evaluation of the diffuseness of synthetic late reverberation created by wave field synthesis at different listening positions," in *DAGA*, Nürnberg, Mar. 2015. [Online]. Available: http://pub.dega-akustik.de/DAGA_2015/data/articles/000169.pdf.

[12] S. Riedel and F. Zotter, "Surrounding line sources optimally reproduce diffuse envelopment at off-center listening positions," *JASA-EL*, vol. 2, no. 9, p. 094 404, 2022. [Online]. Available: https://doi.org/10.1121/10.0014168.

[13] F. Zotter, S. Riedel, L. Gölles, and M. Frank, "Diffuse sound field synthesis: Ideal source layers," *Acta Acustica*, vol. 6, no. 34, p. 16, Sep. 2024. [Online]. Available: https://doi.org/10.1051/aacus/2024023.

[14] F. Zotter, S. Riedel, L. Gölles, and M. Frank, "Diffuse sound field synthesis: Towards practical source layers," *Acta Acustica*, vol. 9, no. 36, p. 16, Jun. 2025. [Online]. Available: https://doi.org/10.1051/aacus/2025018.

[15] T. Tanaka and M. Otani, "An isotropic sound field model composed of a finite number of plane waves," *Acoustical Science and Technology*, vol. 44, no. 4, 2023. [Online]. Available: https://doi.org/10.1250/ast.44.317.

[16] T. Tanaka and M. Otani, "Directionally characterized pseudo-perfect diffuseness: A detailed comparison of its theoretical formulations," *Acoustical Science and Technology*, vol. advpub, e24.16, 2024. [Online]. Available: https://doi.org/10.1250/ast.e24.16.

[17] T. Tanaka and M. Otani, "Spatially characterized pseudo-perfect diffuseness via finite-degree spherical harmonic diffuseness," *JASA Express Letters*, vol. 4, no. 7, p. 071 601, Jul. 2024, ISSN: 2691-1191. [Online]. Available: https://doi.org/10.1121/10.0026466.

[18] F. Melchior, C. Sladeczek, D. de Vries, and B. Frohlich, "User-dependent optimization of wave field synthesis reproduction for directive sound fields," in *124th AES Conv.*, Amsterdam, May 2008. [Online]. Available: http://www.aes.org/e-lib/browse.cfm?elib=14506.

[19] F. Zotter, S. Riedel, L. Gölles, and M. Frank, *Diffuse sound field synthesis*, 2024. arXiv: 2402.11330 [eess.AS]. [Online]. Available: https://arxiv.org/abs/2402.11330.

[20] *Nist digital library of mathematical functions*, https://dlmf.nist.gov/, Release 1.2.5 of 2025-12-15, F. W. J. Olver, A. B. Olde Daalhuis, D. W. Lozier, B. I. Schneider, R. F. Boisvert, C. W. Clark, B. R. Miller, B. V. Saunders, H. S. Cohl, and M. A. McClain, eds.